IEEE Access
Multidisciplinary | Rapid Review | Open Access Journal

Received August 16, 2018, accepted October 5, 2018, date of publication October 12, 2018, date of current version November 8, 2018.

Digital Object Identifier 10.1109/ACCESS.2018.2875492

The Time-Varying Network Patterns in Motor Imagery Revealed by Adaptive Directed Transfer Function Analysis for fMRI

TAO ZHANG[1,2], MENGCHEN LI[1], LI ZHANG[3], BHARAT BISWAL[1,4], DEZHONG YAO[1,5], AND PENG XU[1,5]

[1]MOE Key Laboratory for Neuroinformation, Clinical Hospital of Chengdu Brain Science Institute, University of Electronic Science and Technology of China, Chengdu 611731, China
[2]Center for Mental Health Development and Research, Xihua University, Chengdu 610039, China
[3]School of Applied English, Chengdu Institute, Sichuan International Studies University, Chengdu 611844, China
[4]Department of Biomedical Engineering, New Jersey Institute of Technology, Newark, NJ 07102 USA
[5]Center for Information in Medicine, School of Life Science and Technology, University of Electronic Science and Technology of China, Chengdu 611731, China

Corresponding authors: Bharat Biswal (bbiswal@gmail.com) and Peng Xu (xupeng@uestc.edu.cn)

This work was supported in part by the National Natural Science Foundation of China under Grant 61522105 and Grant 81330032, in part by the Sichuan Science and Technology Program under Grant 2018JY0526, and in part by the Education Department of Sichuan Province under Grant 18SB0596.

ABSTRACT Motor imagery (MI) is a multi-dimensional high-level cognitive ability that involves coordinated contributions from multiple brain regions [i.e., supplemental motor area (SMA), premotor cortex (M1), and posterior parietal cortex] and their couplings as well. However, the dynamic interactions among these activated regions during MI are still unclear. Here, we applied the adaptive directed transfer function (ADTF) to track time-varying connectivity patterns among activated regions during MI. We found that the connectivity patterns are different in two MI tasks and dynamically changes over time, representing special state-dependent and timing-dependent time-varying connectivity patterns. Our findings indicate that left anterior insula (aIns), contralateral SMA, and contralateral M1, which served as important causal targets, play crucial roles in reorganization of the network at different stages, implying that there exists a hierarchical network reorganization during MI. In addition, we found that the lateralization of the left- and right-hand MI occurred in the MI middle stages and was reflected by the effective connectivities modulated by contralateral SMA. Moreover, a graph analysis was adopted to further characterize the temporal evolution of these interactions among activated regions. We also found that network efficiencies are coordinated with the connectivity pattern of networks during MI. Collectively, these findings based on the ADTF analysis expand our understanding of the time-varying network organization in MI.

INDEX TERMS Motor imagery, time-varying network, adaptive directed transfer function, fMRI.

I. INTRODUCTION

Motor imagery (MI) is one important fundamental cognitive ability of the mind. It is generally defined as a dynamic mental rehearsal of a given motor act without any concomitant physical movement [1]. Many studies have shown that MI is beneficial to the improvement of motor skills, rehabilitation of motor function and control of brain-computer interfaces [2]–[5], which have become inseparable parts of people's daily lives [6], [7]. The underlying neural mechanism of MI has been extensively studied from different aspects using various neuroimaging techniques, such as electroencephalogram (EEG) [8], [9] and magnetic resonance imaging (MRI) [10], [11]. The studies have consistently demonstrated that multiple brain regions are activated during MI including the supplementary motor area (SMA), primary motor area (M1), inferior parietal lobule (IPL), putamen, insula, cerebellum and other areas [12]. However, the interactions, especially the dynamic connectivity, among these brain areas are still unclear.

Recently, there has been growing evidence suggesting that the interactions among task-related brain regions are useful for better understanding cognitive processes of the human brain [13]–[15]. Meanwhile, based on those constructed brain networks, multiple network measurements can be obtained and further used in multiple aspects, such as BCI and the diagnose of clinical diseases [16]–[18]. The interactions in

the network are mainly studied with functional or effective connectivity. Functional connectivity is generally defined as the temporal correlations between spatially remote brain regions without the direction of the flow of information [19]. For example, in our previous study [10], by using the resting-state functional connectivity analysis in the fronto-parietal attention network (FPAN), we showed that an effective FPAN network can facilitate MI performance. The effective connectivity is defined as the causal influence that one brain area exerts over another with the direction of the flow of information [20]. Gao *et al.* [21] applied the conditional Granger causality method to measure the effective connectivity between activated regions during MI. They found more circuits of effective connectivity among the task-activated core regions during right-hand MI than during left-hand MI. Kasess *et al.* (2008) used dynamic causal modeling to estimate the effective connectivity between SMA and M1, and the results revealed that the connection from SMA to M1 strongly suppressed the activation of M1 during MI. In addition, Solodkin *et al.* [22] utilized structural equation modeling to study the effective connectivity network among the specified regions of interest (ROIs) during MI, where their results also showed that the connection from SMA to M1 was strong and negative during MI, implying a suppressive effect of SMA on M1.

The aforementioned techniques for estimating the interactions between areas or networks are dependent upon the assumption that the connections remain constant over an entire time course (i.e., 5 minutes or more) [10], [19], [23]. However, the nature of neural activity is highly dynamic even within the resting state, showing evidence of time-varying network connectivity patterns [24], [25]. Therefore, the static connectivity pattern obtained by averaging over the whole period of time is not efficient enough to capture the information regarding network dynamic reconfiguration [26]. Recently, several new methods have been proposed for investigating dynamic connectivity for facilitating understanding of cognitive processes of the human brain at different time scales (i.e., seconds, minutes, years or decades) in the fMRI time course [27]–[29]. For example, Allen *et al.* [30] combined a sliding time window (size $=$ 44 s) and independent component analysis (ICA) to examine dynamic functional connectivity at rest in healthy subjects, resulting in seven states with different network connectivity patterns. Using a similar procedure, they also found dynamic connectivity changes in schizophrenic patients [31]. Deshpande *et al.* [32] applied directed transfer function (DTF) analysis of multivariate Granger causality (GC) to analyze dynamic effective connectivity changes of the network (three time windows) in motor fatigue, revealing dynamic evolution of the motor network during the fatigue process. In addition, Monti *et al.* [25] proposed a Smooth Incremental Graphical Lasso Estimation (SINGLE) algorithm to estimate the dynamic interactions of network at a higher temporal granularity. Based on this new method, they found that the right inferior frontal gyrus (IFG) and right IPL played important roles in regulating the dynamic balance between other brain regions in attention and execution tasks. From another aspect, Liu and Duyn [33] proposed a single-volume co-activation pattern analysis method to reveal multiple spatial patterns at a single time point. In sum, these findings consistently imply that the dynamic interactions of network analysis provide a new method for better understanding the nature of the human brain.

Although these dynamic connectivity analysis methods enriched our knowledge of the functional organization of the brain, one of the main issues associated with their practical use is that the choice of the optimal window size or interesting observations is actually difficult, which requires experience or the complicated evaluation procedure [25]. Recently, several methods have shown higher efficiencies for estimating time-varying connectivity, such as time-varying GC (tv-GC), time-varying partial directed coherence (tv-PDC), and adaptive directed transfer function (ADTF), also named time-varying DTF (tv-DTF), all of which are defined in the frequency domain and are based on the use of a time-varying multivariate adaptive autoregressive (tv-MVAAR) model built on original time series [34]–[36]. These time-varying methods can not only identify a time-variant network pattern at each single time point without the additional requirement of choosing the window size but also capture the direction of the functional coupling (information propagation). Therefore, they have been widely used for time-varying network analysis for electrophysiological signals including EEG and Ecog [37], [38]. For example, Samdin *et al.* [39] applied tv-PDC and ADTF to the MI-EEG data to investigate dynamic interactions among motor areas, and they found that the event-related changes of information flows around the beta-band in a unidirectional way between the left and right hemisphere during MI. Wilke *et al.* [36] also reported that the ADTF can reconstruct the time-varying connectivity patterns consistent with the real epileptic-form electrocorticogram (EcoG) data that come from an epilepsy patient. Moreover, in the study of P300, Li *et al.* [40] used ADTF to reveal that the various P300 stages (i.e., the decision process and neuronal response stages) correspond to different brain network structures. These findings demonstrated that these time-varying methods seem to be a good tool for investigating dynamic network patterns and directional information flow at shorter time scale. However, these techniques to date have primarily applied to high time resolution EEG data, and very few studies have used such methods in MRI data.

In the present study, we applied ADTF and graph analysis to explore the neural mechanism of MI based on MI fMRI data. First, general linear model (GLM) analysis was used to acquire the activated regions during left- and right-hand MI, respectively. Subsequently, the ADTF was used to estimate time-varying network connectivity based on these task-activated ROIs during two MI tasks. Finally, the graph analysis was used to quantitatively evaluate the time-varying network properties, which will characterize the different

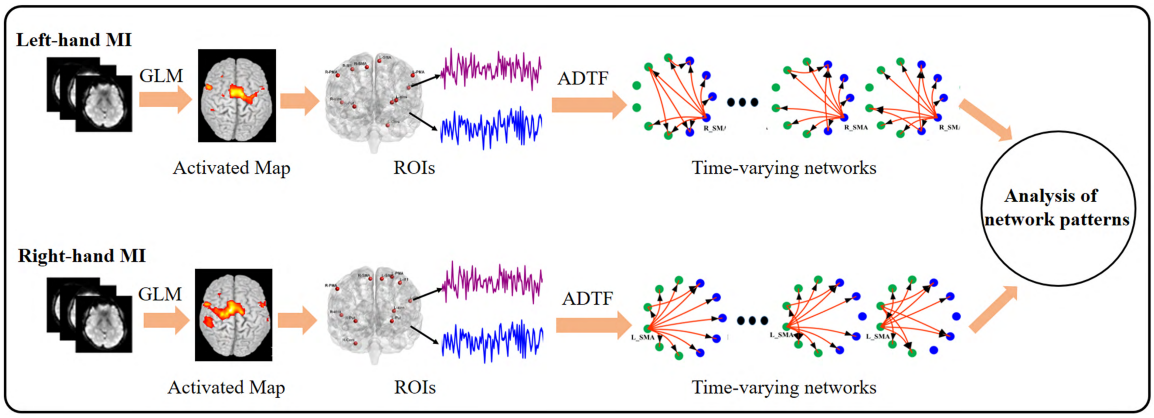

FIGURE 1. An analytical process of time-varying network connectivity.

strategies used in the different MI states for information processing.

II. MATERIALS AND METHODS

A. SUBJECTS

Twenty-six healthy university students were recruited (9 females and 17 males, aged 22.85 ± 2.48 years, range 19-26 years, 24 right hand-dominant) to complete the MRI scanning. All participants did not habitually consume drugs and alcohol, and had no cognitive impairments or neurological disorders. Two left-handed subjects and four subjects with large head motion were excluded. The experimental protocol was approved by the Institutional Research Ethics Board of the University of Electronic Science and Technology of China (UESTC). All participants were asked to read and sign an informed consent form before participating in the study.

B. EXPERIMENTAL DESIGN AND PROCEDURES

The fMRI experiment consisted of four runs: one left-hand MI task, one left-hand motor execution (ME) task, one right-hand MI task, and one right-hand ME task. Each run included 20 blocks, and each block lasted 40 s including 2 s cue, 20 s task and 18 s rest. Each block, begins with a 2 s yellow fixation cross in the center of the screen to indicate subjects to prepare for the following task. Then, the color of the yellow fixation cross turned white and a gray left or right arrow also appeared on the screen, and subjects were asked to perform motor imagery (executive) during the 20 s period. During MI, all participants were conducted to performance sustained kinesthetic imagery. When the arrow disappeared, subjects were allowed to have 18 s rest while being asked to still focus their attention on the gray fixation cross. In this study, we only considered the left- and right-hand MI tasks.

C. MRI DATA ACQUISITION

Functional imaging was performed at the medical center of UESTC using a GE 3T scanner with an eight channel-phased array head coil. Functional images were collected using a single-shot echo-planar imaging (EPI) sequence (TR = 2000 ms, TE = 30 ms, flip angle = 90ř, matrix size = 64 × 64, field of view (FOV) = 24 × 24 cm^2, slice thickness/gap = 4 mm/0.4 mm, and 32 slices oriented in an AC-PC line).

D. ANALYSIS PROCEDURE

A block diagram of the data analysis procedure is shown in Fig. 1 First, the MI task-related fMRI data were preprocessed. Second, the GLM analysis was applied to obtain individual and group task-related t-contrast images. Third, group analysis results were used to extract the regions of interest (ROIs). Fourth, the ADTF method was used to construct the time-varying network for two MI tasks. Finally, graph analysis and time-varying network analysis were conducted to investigate the dynamic patterns of network connectivity for MIs. Detailed information regarding these steps is described in the following sections.

E. FMRI DATA PREPROCESSING

The preprocessing analysis was performed using the statistical parametric mapping software (SPM8; http://www.fil.ion.ucl.ac.uk/spm). All functional runs were preprocessed following a standard pipeline of slice scan-time and 3D motion correction, normalization to the Montreal Neurological Institute (MNI) space with the EPI template, and smoothed with a 6 mm FWHM Gaussian kernel.

F. MI TASK-INDUCED ACTIVATION ANALYSIS

In the current study, activation analysis was performed, aiming to validate these MI tasks and to extract a set of task-related ROIs to be used for subsequent time-varying network analysis. For each subject, task-related fMRI data were first entered in a first level linear model in SPM8. The MI task onsets and six head motion parameters constituting the design matrix are modeled as regressors convoluted by a canonical HRF. In addition, the data were further processed by temporally filtering with a high-pass filter (cut-off of 128 s) and no global scaling. Then, t-statistic was performed to calculate

TABLE 1. MNI coordinates and t-values of significantly activated regions for both the right- and left-hand MI tasks.

Regions	Hem	BA	Right-hand MI			t-value	Left-hand MI			t-value
			x	y	z		x	y	z	
M1	L(R)	4	-36	-15	54	4.13	33	-12	54	6.0
IPL	L	6/40	-51	-30	27	5.57	-48	-39	27	4.2
Cere	R(L)		30	-42	-36	5.13	-18	-45	-27	4.22
SMA	L	6	-9	-6	60	10.83	-6	-6	66	8.77
	R	6	8	-3	60	6.27	12	-6	57	8.63
PMA	L	6	-24	-15	63	8.65	-54	6	45	4.43
	R	6	57	6	45	5.86	54	6	45	3.9
Put	L		-24	-3	-3	4.95	-24	-12	6	5.45
	R		30	-3	-3	4.06	30	-6	0	6.51
aIns	L		-27	-24	12	4.06	-30	30	9	5.62
	R		51	5	6	5.31	48	3	6	5.17

Abbreviations: BA = Hem = hemisphere, Brodmann's area, L = left, R = right, M1 = primary motor area, IPL = inferior parietal lobule, Cere = cerebellum, SMA = supplementary motor area, PMA = premotor area, Put = Putamen, aIns = anterior insula. Voxel coordinates are the MNI coordinates of the ROI center.

the individual task-related t-contrast images (MI $>$ 0). After that, a one-sample t-test was performed to examine the group level effects for MIs based on the individual t-contrast maps. These statistical maps were corrected for multiple comparisons at the voxel level using a false discovery rate (FDR, $p < 0.05$). Finally, the local peaks were assessed to define ROIs for further time-varying network analyses.

G. REGIONS OF INTEREST

The aim of the current study was to explore the time-varying network connectivity among the key activated areas involved in our MI experimental tasks. Considering that the definitions (i.e., prior brain atlas, task scanning or independent component analysis) of ROIs can have a large influence on the patterns of network connectivity and the properties of network topology [41], task-based definition operated as an important method was selected in this study [42], [43]. According to the local peaks in the MI-task $>$ 0 t-contrast of the group analysis, a total of 11 ROIs were defined for the left- and right-hand MI, respectively. For different MI-task conditions in particular, we selected the contralateral M1 and ipsilateral cerebellum (Cere) corresponding to the MI-related performing hand. The MNI coordinates and their corresponding nomenclatures and T-values for these 11 ROIs are listed in Table 1. All ROIs were defined as spheres with 6 mm radius. The averaged time course of each ROI was then extracted for two MI conditions for each subject. These time courses were used for further analyses

H. CONSTRUCTION OF MI-RELATED TIME-VARYING FUNCTIONAL BRAIN NETWORK

A brain functional network contains two basic elements: a set of nodes and edges. Nodes can be denoted with activated ROIs, and edges can be defined by the coupling relationships between pairs of nodes. Based on the extracted time course of the ROIs, we constructed a time-varying dynamic network for left- and right-hand MI for each the concerned time point, respectively. The construction of the time-varying network was composed of four main steps: (1) MI-task fMRI data segmentation, (2) tv-MVAAR model coefficient estimation, (3) ADTF values calculation, and (4) dynamic network pattern estimation. Detailed descriptions of these steps are shown in the following sub-sections.

1) DATA SEGMENTATION

To identify the transient architecture of the network during MI, we mainly focused on a complete MI process. Since the MI experiment is a block design, the same task was repeated in each block. In our study, the MI-task was scanned for 400 time points, including 20 blocks. The MI-related fMRI time series were segmented in the interval [1]–[20] TR (2-40s) according to the onset of the MI task. Finally, these block-by-block time courses were then used to construct a dynamic network using ADTF.

2) IDENTIFICATION OF THE TV-MVAAR MODEL BY KALMAN FILTER

In order to calculate the ADTF values, the tv-MVAAR model [44]–[46] is first formed based on the time courses of the extracted ROIs. Let a single block time course $X(t) = (x_1, x_2, \ldots, x_{20})$ be the data vector with 20 time points. Then the tv-MVAAR model is obtained for left- and right-hand MI task blocks by the equation

$$X(t) = \sum_{i=1}^{p} A(i,t)X(t-i) + E(t) \quad (1)$$

where $A(i,\ t)$ represents the coefficient matrix of the tv-MVAAR model, which is estimated by the Kalman filter algorithm [20], [47], $E(t)$ is the multivariate independent white noise process, and p is the corresponding model order, which is automatically determined using the Akaike Information Criterion (AIC) [48].

3) ADTF VALUE CALCULATION AND TIME-VARYING NETWORK PATTERN ESTIMATION

By transforming equation (1) to the frequency domain, we can obtain the ADTF function $H(f, t)$. Based on the coefficient matrix of the tv-MVAAR model, $A_{k,}$, the ADTF is calculated [36] by

$$A(f, t)X(f, t) = E(f, t) \tag{2}$$

$$X(f, t) = A^{-1}(f, t)E(f, t) = H(f, t)E(f, t) \tag{3}$$

where $A(f, t) = \sum_{k=0}^{p} A_k(t)e^{-j2\pi f \Delta tk}$, and $X(f,\ t)$ and $E(f,\ t)$ are the corresponding transformations of $X(t)$ and $E(t)$ in the frequency domain.

The function $H(f,\ t)$ contains all the information of the spectral properties and the interactions between ROIs and the element H_{ij} in $H(f,\ t)$ represents the directed information flow from ROI j-th to$i$-th at time point t. Then, the normalized ADTF is defined between [0, 1] as,

$$\gamma_{ij}^2(f, t) = \frac{\left|H_{ij}(f, t)\right|^2}{\sum_{m=1}^{n} |H_{im}(f, t)|^2} \tag{4}$$

To evaluate the total information flow from a single ROI, the integrated ADTF is calculated [36] by averaging the ADTF values over the all interested frequency band (0.01-0.1Hz) that is considered to be meaningful in the BOLD signal,

$$\Theta_{ij}^2(t) = \frac{\sum_{k=f_1}^{f_2} \gamma_{ij}^2(k, t)}{f_2 - f_1} \tag{5}$$

Based on the frequency band of interest, the time-varying network was constructed for each block. Finally, the block-by-block connectivity patterns were estimated by averaging over all the blocks for each time point for each subject. To reveal the common time-varying network patterns for all the subjects, the time-varying networks were further averaged across all subjects at each concerned time point.

I. SIMULATED SIGNALS

In the present study, to evaluate the availability of ADTF to capture the time-varying connectivity patterns, we initially applied ADTF to the simulated data. We predefined three directed network models (see Fig. 3b) with four nodes to simulate the different patterns in the different time periods. The three network patterns are specifically described as follows:

For the first phase, t from 1 to 10s.

$$\begin{aligned}
\mathrm{X}(1, \mathrm{t}) &= \varepsilon(1, \mathrm{t}) - 0.25\mathrm{X}(1, \mathrm{t}-1) + 0.30\mathrm{X}(2, \mathrm{t}-2) \\
\mathrm{X}(2, \mathrm{t}) &= \varepsilon(2, \mathrm{t}) + 0.20\mathrm{X}(2, \mathrm{t}-1) \\
\mathrm{X}(3, \mathrm{t}) &= \varepsilon(3, \mathrm{t}) + 0.25\mathrm{X}(3, \mathrm{t}-1) + 0.30\mathrm{X}(2, \mathrm{t}-2) \\
\mathrm{X}(4, \mathrm{t}) &= \varepsilon(4, \mathrm{t}) - 0.25\mathrm{X}(4, \mathrm{t}-1) + 0.30\mathrm{X}(2, \mathrm{t}-2)
\end{aligned} \tag{6}$$

For the second phase, t from 11 to 20s.

$$\begin{aligned}
\mathrm{X}(1, \mathrm{t}-100) &= \varepsilon(1, \mathrm{t}-100) - 0.10\mathrm{X}(1, \mathrm{t}-101) \\
&\quad + 0.90\mathrm{X}(2, \mathrm{t}-102) \\
\mathrm{X}(2, \mathrm{t}-100) &= \varepsilon(2, \mathrm{t}-100) + 0.20\mathrm{X}(2, \mathrm{t}-101) \\
\mathrm{X}(3, \mathrm{t}-100) &= \varepsilon(3, \mathrm{t}-100) - 0.10\mathrm{X}(3, \mathrm{t}-101) \\
&\quad + 0.90\mathrm{X}(4, \mathrm{t}-102) \\
\mathrm{X}(4, \mathrm{t}-100) &= \varepsilon(4, \mathrm{t}-100) - 0.10\mathrm{X}(4, \mathrm{t}-101) \\
&\quad + 0.90\mathrm{X}(2, \mathrm{t}-102)
\end{aligned} \tag{7}$$

For the third phase, t from 21 to 30s.

$$\begin{aligned}
\mathrm{X}(1, \mathrm{t}-200) &= \varepsilon(1, \mathrm{t}-200) - 0.10\mathrm{X}(1, \mathrm{t}-201) \\
&\quad + 1.40\mathrm{X}(4, \mathrm{t}-202) \\
\mathrm{X}(2, \mathrm{t}-200) &= \varepsilon(2, \mathrm{t}-200) - 0.10\mathrm{X}(2, \mathrm{t}-201) \\
&\quad + 1.40\mathrm{X}(4, \mathrm{t}-202) \\
\mathrm{X}(3, \mathrm{t}-200) &= \varepsilon(3, \mathrm{t}-200) - 0.10\mathrm{X}(3, \mathrm{t}-201) \\
&\quad + 1.40\mathrm{X}(4, \mathrm{t}-202) \\
\mathrm{X}(4, \mathrm{t}-200) &= \varepsilon(4, \mathrm{t}-200) + 0.20\mathrm{X}(4, \mathrm{t}-201)
\end{aligned} \tag{8}$$

where X denotes the time series on the four network nodes, which conforms to normal distribution. Using this model, the corresponding four simulated signals for these nodes were generated, which contained 100 trials to simulate actual repeated stimuli in fMRI experiment. After the trials are generated, the Gaussian noise with different SNRs (0, 5 and 10 dB) is added. We then evaluated the tvMVAAR coefficients for each single-trial. Finally, based on the mean tvMVAAR coefficients across all trials, we constructed the time-varying networks using ADTF.

J. MI-RELATED TIME-VARYING BRAIN NETWORK PROPERTIES

Depending on the state condition of the brain (i.e., task or resting state), the network connectivity patterns (i.e., strength or information flow) can affect the efficiency of the network. Graph analysis provides an important method to measure the efficiency of the network. In this study, four common directed weighted network properties including the clustering coefficient (C), global efficiency (Ge), local efficiency (Le), and characteristic path length (L), were calculated for each time-varying network using the brain connectivity toolbox (http://www.nitrc.org/projects/bct/) [49], [50]. Detailed definitions of these network measurements are

shown as follows:

$$C = \frac{1}{n}\sum_{i\in N} \times \frac{\frac{1}{2}\sum_{j,h\in N}(w_{ij}+w_{ji})(w_{ih}+w_{hi})(w_{jh}+w_{hj})}{(\sum_{j\in N} w_{ij}+\sum_{j\in N} w_{ji})(\sum_{j\in N} w_{ij}+\sum_{j\in N} w_{ji}-1)-2\sum_{j\in N} w_{ij}w_{ji}} \quad (9)$$

$$L = \frac{1}{n}\sum_{i\in N}\frac{\sum_{j\in N, j\neq i} d_{ij}^{\rightarrow}}{n-1} \quad (10)$$

$$Ge = \frac{1}{n}\sum_{i\in N}\frac{\sum_{j\in N, j\neq i}\left(d_{ij}^{\rightarrow}\right)^{-1}}{n-1} \quad (11)$$

$$Le = \frac{1}{2n}\sum_{i\in N} \times \frac{\sum_{j,h\in N, j\neq i}(w_{ij}+w_{ji})(w_{ih}+w_{hi})\left(\left[d_{jh}^{\rightarrow}(N_i)\right]^{-1}+\left[d_{hj}^{\rightarrow}(N_i)\right]^{-1}\right)}{(\sum_{j\in N} w_{ij}+\sum_{j\in N} w_{ji})(\sum_{j\in N} w_{ij}+\sum_{j\in N} w_{ji}-1)-2\sum_{j\in N} w_{ij}w_{ji}} \quad (12)$$

where w_{ij} is a weighted connection strength between node i and j, $d_{ij}^{\rightarrow}$ is the shortest directed path length between node i and j. N is the set of network nodes, n is the number of nodes. For more details on these network properties, please refer to previous literature [49], [50].

In addition, the in-degrees and out-degrees of the nodes were also calculated for each task to evaluate the time-varying causal interactions of each node [21].

III. RESULTS

A. BRAIN ACTIVATION DURING LEFT- AND RIGHT-HAND MI

In order to identify specific ROIs for the subsequent time-varying brain network analyses, we evaluated the brain activities that were elicited by different MI tasks. Fig. 2 showed the brain activation during left-hand MI (Fig. 2a) and right-hand MI (Fig. 2b) obtained with the group analysis (t-statistic). The contrast of left-hand MI (task $>$ 0) generated a set of clusters with local maximum peaks, including bilateral SMA, PMA, Putamen, aIns, and left Cere, left IPL and right M1 (see Table 1). Similarly, the contrast of right-hand MI (task $>$ 0) generated a set of clusters with local maximum peaks, including the bilateral SMA, PMA, Putamen, aIns, and right Cere, left IPL and left M1 (see Table 1).

B. EVALUATION OF THE ADTF MODEL WITH SIMULATED DATA

To evaluate the availability of ADTF to capture the time-varying network patterns, artificial data was used. Fig. 3a showed the simulated time series in the three phases for each node. Fig. 3b showed the three predefined network connectivity patterns. By using ADTF, we can estimate the dynamic

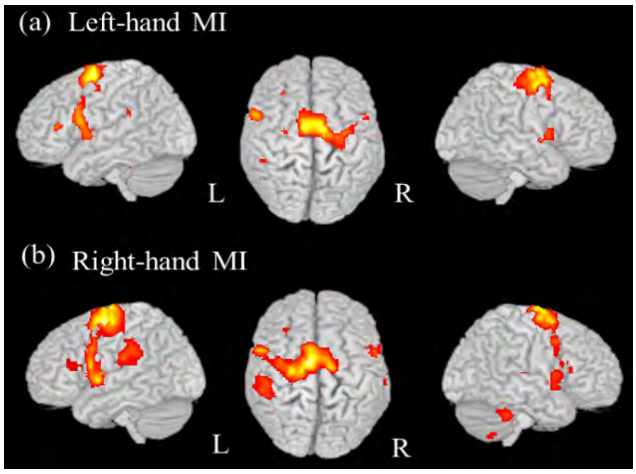

FIGURE 2. The activated areas during left-hand MI and right-hand MI by group analysis. (a) The activated areas during left-hand MI ($p < 0.05$, FDR, t-value > 3.3). (b) The activated areas during right-hand MI ($p < 0.05$, FDR, t-value > 3.5).

network processes at the concerned time point (i.e., every 2 seconds). Fig. 3c showed the estimated tvMVAR coefficients for our predefined network patterns under three different noise conditions, where we found that ADTF can effectively track fluctuation trends of coefficients that are determinative for the time-varying network construction. Based on the estimated time-varying coefficients, the corresponding time-varying networks could be constructed, and the networks at every 2 seconds (i.e., TR $=$ 2 seconds) for each stage are given in Fig. 3d. The results suggested that the ADTF is available to capture the dynamic network pattern at a relatively shorter time scale, which is important to probe the underlying mechanism of information processing for cognitive processes.

C. TIME-VARYING NETWORK PATTERNS OF LEFT- AND RIGHT-HAND MI

To provide an intuitive comparison, we kept the strongest 10% of directed connections of each state (i.e., one time point) to clearly show the divergent (dynamic) connectivity pattern among states based on the group averaged time-varying networks [51], [52]. In the current study, we mainly focused on the cue and MI-task states (total of 11 states). Fig. 4 showed the time-varying network patterns for the cue and left- and right-hand MI.

During left-hand MI, in the cue state, we found that the left aIns, IPL and right aIns have more interactions with other regions. In states 1 and 2, the interactions (more connections) were increased in the left aIns, whereas the interactions were decreased in the left IPL and right aIns. In state 3, the right M1 shifted to a new 'hub' with more connections. In state 4, the right M1 lost its 'hub', whereas the right SMA instead became a new 'hub'. States 5-10 share a similar network pattern such that the right SMA is an important causal outflow source for modulating other regions. In addition, we also observed in these states that more connections existed in the

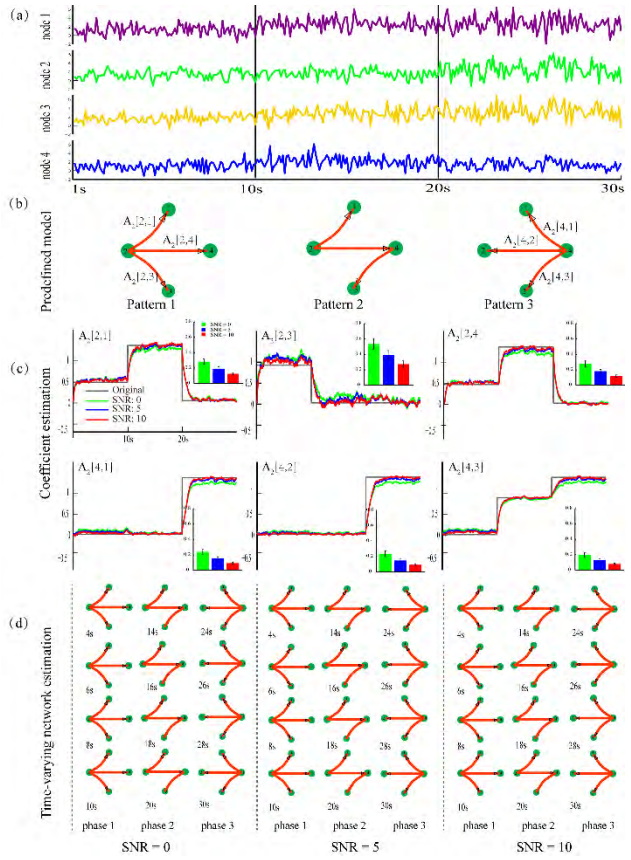

FIGURE 3. Estimation of time-varying networks based on simulated data using the ADTF. (a) The simulated signals in a trial for each node. (b) Three predefined network connectivity model in the different stages. Ap[ni,nj] is the (ni,nj)-th entry of the tvMVAR coefficient matrix, and it represents the causal influence of node nj on ni. (c) The estimated tvMVAR coefficients for 0dB, 5dB and 10dB noise SNRs. The gray line denotes the true tvMVAR coefficient. The green, bule and red line represent the tvMVAR coefficients estimated under different SNRs. In addition, the coefficients errors are given for each noise condition by the color bars. (d) Time-varying networks patterns estimated using ADTF for different time stages under three noise conditions.

right hemisphere contralateral to the left-hand MI, especially interactions in the right SMA.

During right-hand MI, in the cue state, we found that the left aIns and PMA have more interactions with other regions and that the left IPL and right aIns are also important nodes for receiving information. In states 1-3, we found that they share a similar network pattern with the left aIns, PMA and M1 playing important roles in network interactions. These states, however, still own unique connections patterns across time, i.e., the interactions in the left aIns were gradually weakened, whereas the interactions in the left M1 were gradually strengthened from state 1 to 3. In state 4 compared to state 3, the left PMA shows increased interactions, whereas the left M1 shows decreased interactions. In state 5, almost all the interactions are connected with the left PMA and SMA, and the left M1 uniquely receives information coming from the left PMA and SMA. In states 6-8, the left SMA serves as a 'hub', which is an important information source to modulate almost all the interactions within the network. States 9 and 10 have a similar network pattern with the cue state such that the left PMA and aIns play hub-like roles in the network. In the time-varying network patterns, we also observed that dense connections existed in the left hemisphere contralateral to the right-hand MI, especially interactions in the left SMA. Besides the 10% cost, we also investigated the time-varying network patterns under other cost values like 5% and 15%, and found the similar patterns as that in Fig. 4.

D. TIME-VARYING MI NETWORK PROPERTIES

To better understand the evolution patterns of the time-varying networks, the four global network properties (i.e., C, L, Ge, and Le) were calculated for each state for each subject. Fig. 5 shows the time-varying network properties for the left- and right-hand MI averaged across subjects. We found that the network properties (i.e., C, Ge, and Le) were gradually increased, and the network property (L) was gradually decreased in states 1-6. These time-varying network properties collectively indicated that the network efficiency gradually increases to satisfy the requirement for MI-related information processing. During the last 5 states, all the network properties were relatively stable in both MI tasks. In addition, we also found that the network efficiency of right-hand MI is higher than that of left-hand MI at the beginning of several states.

E. IN- AND OUT-DEGREES OF NODES IN THE TIME-VARYING NETWORK

Fig. 6 shows the in- and out-degrees of nodes in the time-varying network for the left- and right-hand MI, respectively. During left-hand MI, the left aIns and right SMA have relatively higher out-degrees at different periods (Fig. 6a). The in-degrees of all nodes are kept relatively smooth, and the left IPL and right aIns have relatively higher in-degrees over time (Fig. 6c). During right-hand MI, the left aIns, PMA and SMA have relatively higher out-degrees at different periods (Fig. 6b). Similar to left-hand MI, the changes of the in-degrees of all nodes are relatively smooth, and the left IPL, left M1 and right aIns have relatively high in-degrees over time (Fig. 6d). To further explore the interactions between the left and right hemispheres during two MI tasks, we calculated the average out-degree of the regions within the right hemisphere, which only connected with the left hemisphere regions for the left-hand MI, and the averaged out-degree of the regions within the left hemisphere, which only connected with the right hemisphere regions for the right-hand MI. In other words, we estimated the network causal influence strength between two hemispheres to evaluate the lateralization of left- and right-hand MI. Fig. 6e showed the averaged lateralization strength of left- and right-hand MI over time. We found that the causal influence of the left hemisphere regions exerted on the right hemisphere regions is relatively stable over time during right-hand MI, whereas the causal influence of the right hemisphere regions exerted on the left

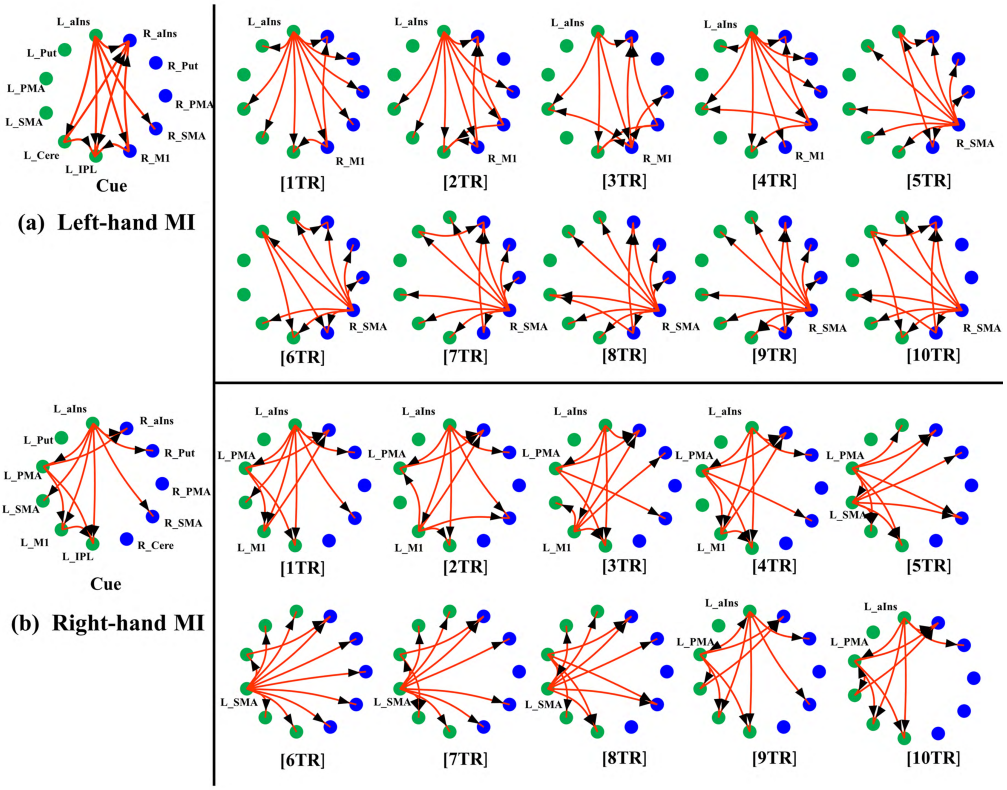

FIGURE 4. Time-varying networks estimated by ADTF. (a) The time-varying networks for the left-hand MI. (b) The time-varying networks for the right-hand MI. Green dots represent areas in the left hemisphere. Blue dots represent areas in the right hemisphere. Red lines indicate the synchronous coupling between two ROIs, and arrows indicate the direction of their information flow.

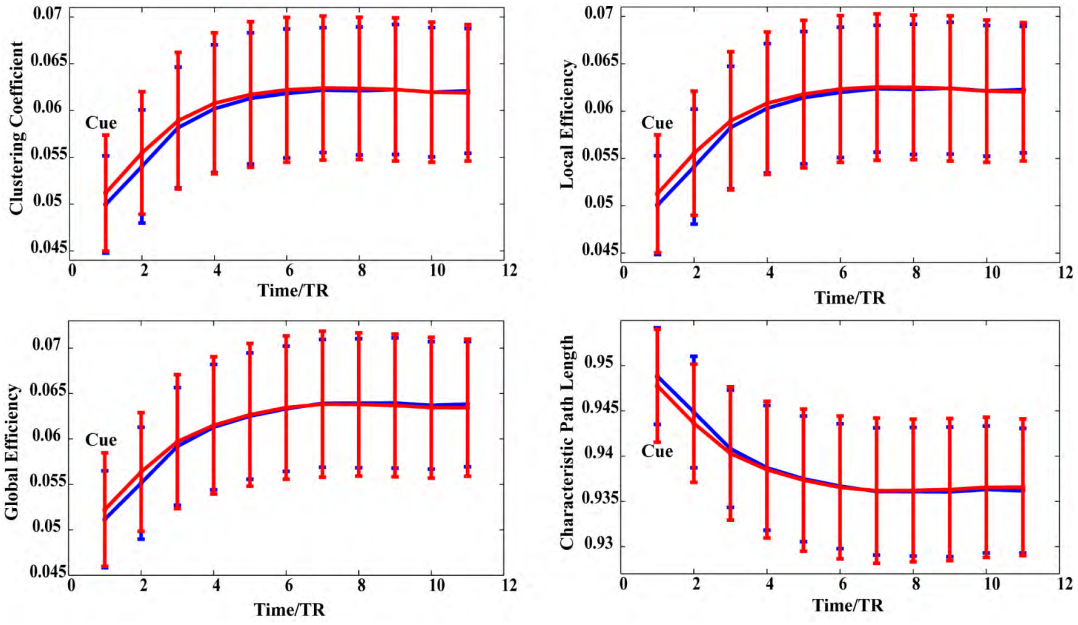

FIGURE 5. Time-varying network properties for the left- and right-hand MI. Blue and red lines represent the corresponding network properties of left- and right-hand MI tasks, respectively.

hemisphere regions is gradually increased over time during left-hand MI. Moreover, during states 7-11, much stronger causal influence from right to left hemisphere is observed for the left-hand MI when compared to the right-hand MI with relatively weaker causal influence from left to right hemisphere.

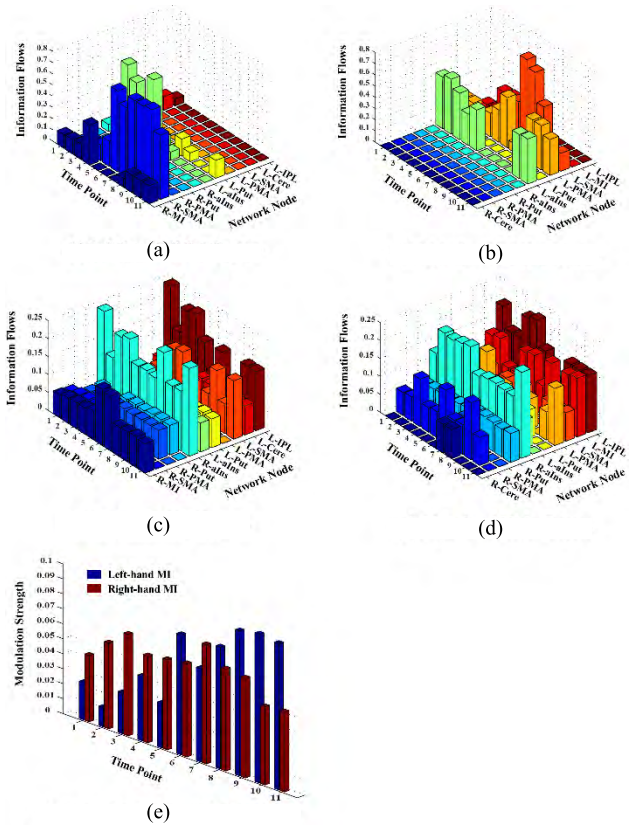

FIGURE 6. The in-degree and out-degree for each node. (a) and (c) are the in- and out-degrees of nodes of time-varying network during left-hand MI. (b) and (d) are the in- and out-degrees of nodes of time-varying network during right-hand MI. (e) Causal influence between two hemispheres for left- and right-hand MI.

IV. DISCUSSION

In the current study, ADTF, which has the capability to estimate the time-varying effective connectivity at each time point, was successfully applied to the fMRI data to explore the dynamic interactions in activated regions involved in MI. Our results revealed that SMA, aIns, and M1 play important roles in dynamic interactions of the network at different task periods and showed a significant hemispheric lateralization of the dynamic connectivity during left- and right-hand MI, especially in the connections from the contralateral SMA to other regions. Our findings demonstrated that ADTF serves as an effective tool that can provide novel insights into dynamic interaction processes during MI tasks.

A. METHODOLOGICAL CONSIDERATIONS

To the best of our knowledge, this is the first study to apply ADTF to fMRI data to explore time-varying directed interactions among regions. Such time-varying connectivity patterns were enabled by incorporating the Kalman filter algorithm into the tv-MVAAR model [36]. This method has been widely used in the EEG fields to study the time-variant propagation of brain activity, indicating that it is a useful tool to construct time-varying networks during various cognitive processes [36], [53]. Compared to other time-varying analysis methods mainly based on the sliding window strategy, ADTF can identify the time evolution process of the network connectivity patterns at each time point rather than over the entire time course or in a coarser sliding window. This allows for quantifying the dynamic behavior of the networks at a shorter time scale. As shown in Fig. 3a and b, three different network structures are hidden in the simulated signals. Without any prior interference such as the time window selection, ADTF used the Kalman filter to automatically estimate the connectivity patterns at each time point. In essence, ADTF constructs the time-varying networks based on the MVAR coefficients, that is to say, the accurate estimation of the corresponding MVAR coefficients is critical to capture the dynamic network structures. The estimated time-varying MVAR coefficients in network patterns in Fig. 3c reveal that ADTF could actually track the coefficients robustly, where the fundamental fluctuation trends could be captured under different concerned noise conditions. Therefore, based on the accurately estimated MVAR coefficients, and Fig. 3d demonstrated that ADTF is capable of identifying the three predefined dynamic connectivity patterns of the network. These simulation signals follow a Gaussian distribution, which is usually assumed to be the dominant distribution in fMRI data. Moreover, in another simulation study by Wilke *et al.* [36], they also found that ADTF is able to reconstruct various time-variant connectivity patterns, including Gaussian functions, step functions, and oscillating function. Combining our simulation study and previously reported results, we applied ADTF to extract the MI related time-varying networks from fMRI.

As is known, the fMRI response is reflected via the hemodynamic response, which is sluggish and typically takes 6-10s. Indeed, this is in line with the nature of persistent neural representations [54]–[56], especially in the MI task that contains multiple stages such as motor selection, motor planning and motor preparation [57]. Although such slow dynamics, the network model is sensitive to persistent and ramping activity. Thus, ADTF may capture the subtle changes in the network pattern over time. Based on this method, we found some interesting results as described below.

B. BRAIN ACTIVATION OF LEFT- AND RIGHT-HAND MI

Fig. 2 showed the activated regions during two different types of MI. The results are in line with those of many other previous studies [12], [21], [58], [59] and confirmed the significant excitation of the contralateral M1 and ipsilateral Cere corresponding to the performing of MI task [12], [60], [61]. According to different MI conditions, the consistent ROIs in the bilateral SMA, PMA, Putamen, aIns, and left IPL were selected for network analysis, except for M1 and Cere (see Table 1). In the present study, the time-varying inter-regional interactions of the activated regions recruited by MI tasks were further explored using ADTF and graph theory.

C. DYNAMIC INTERACTIONS OF AINS DURING MI

Many studies have indicated that the insula is involved in a wide array of cognitive processes, including focal attention [62], [63], goal-oriented control, switching between networks, conscious awareness of sensations and movements [64], motor imagery [12], cognitive choices and intentions, emotion [65], [66], etc. In fact, the insula has been the topic of considerable neuroscience research and has long been considered to be important in the generation of subjective feelings that guide decision making [67]. In this study, our results showed that regardless of the left- and right-hand MI, the left aIns has always been a core node acting as a 'causal outflow hub' [68], which has a strong casual influence on other regions at state start-cue and task related states 1-4. However, the right aIns mainly acts as a 'causal inflow hub' at the corresponding state conditions to receive the information sent from other related areas. In our MI experiment, before the task begins, the participants were instructed to perform a specific imaginary action of the hand according to the visual arrow indicated cue. In terms of the time-varying connectivity patterns, we found that the left aIns might serve as the first cortical target of interoceptive input [69] during MI. Thus, we suggested that the dynamic interactions between the left aIns and other regions contribute to guide decision making and coordinate network resources.

Although the left aIns is an important causal resource during early MI stage, the causal influence of left aIns exerted on other regions is gradually weakened with the decreased connections. During the later stage of MI, the network center (causal resource) is shifted from the left aIns to other regions (i.e., SMA or PMA). In addition, especially in the last two states, the left aIns connectivity patterns stay relatively stable during left-hand MI, whereas the left aIns connectivity patterns tend to be the state start-cue to become a 'causal outflow hub' during right-hand MI. Given that most of the participants are right-handed in our study, our results indicated that the network architecture of left-hand MI is more stable than that of right-hand MI. In other words, state switching (from task to rest) is easier for right-hand MI, indicating that the subjects can anticipation what is going to happen, which is formed during repeated daily life exercise [70].

D. DYNAMIC INTERACTIONS OF M1 DURING MI

It is clearly indicated that the M1 is actually implicated in MI processes [71], [72]. In our study, we observed that right M1 was activated during left-hand MI, whereas left M1 was activated during right-hand MI, which are in accordance with previous studies [21], [71], [73]. Thus, the contralateral M1 was selected as a ROI to investigate the interactions of time-varying networks. The investigation of time-varying connectivity may provide new insights into the roles of M1 during MI.

The time-varying connectivity patterns showed that, regardless of the left- and right-hand MI, the contralateral M1 played a key role in the early MI period, such as in states 1-3 during left-hand MI and states 1-4 during right-hand MI. In these states, we observed that M1 not only is a causal inflow node but also a causal outflow node in both MI tasks. The causal inflow information comes from the left aIns, such as the causal connectivity from left aIns to contralateral M1, whereas the causal outflow information is mainly exerted on the left IPL and right aIns. These findings implied that M1 may be more sensitive than other regions toward decoding stimulus related information (i.e., movement intention). For example Hochberg *et al.* [74] reported that the utilization of the cortical spiking patterns of M1 can precisely decode the intention of the hand motion in a tetraplegic human.

Moreover, at the later stage of MI, M1 becomes a causal inflow node particularly in right-hand MI. According to the time-varying connectivity patterns, we found that there exists a causal connection from ipsilateral SMA to ipsilateral M1 (i.e., left SMA to left M1) but no feedback between them. Several studies have shown that the MI and ME share some common regions including SMA, PMA and M1 [61], [75], [76]. These brain areas are known to play key roles in the planning, preparation and execution of motor commands [57]. Although these areas were activated in both tasks, the causal connectivity between the SMA and M1 is very different during ME and MI. For example, in a study by Kasess *et al.* [61], they found that the SMA exerts an inhibitory influence on M1 during MI, whereas the influence of SMA on M1 was enhanced during ME. In addition, similar results were also found in amputees [73] and stroke patients [75]. When compared to the time-varying causal connections, these findings also suggested that there exists a suppressive influence of SMA (contralateral) on M1 (contralateral) during both MI tasks at the later stage of MI. Therefore, our results not only confirmed the role of the causal connectivity between the SMA and M1 but also extended previous studies on their interactions.

E. DYNAMIC INTERACTIONS OF SMA DURING MI

Previous studies had indicated that the left and right SMAs played different functional roles in linking cognition to action [77] and reported that there exists an anatomical reciprocal connection between them. Moreover, both the left and right SMAs are projected to M1 [78], [79]. These findings provided strong support for dividing SMA into left and right two parts. More interestingly, beginning from the fifth state, our results showed that the SMAs shifted to a prominent causal outflow hub corresponding to performing MI tasks (i.e., right SMA for left MI and left SMA for right MI). These findings implied that the roles of SMAs are different during two MI tasks and demonstrated that the hemispherical lateralization occurred not only in neural activity (see Fig. 2) but also in the time-varying connectivity networks.

However, in this study, the lateralization is different from that in a previous study by Gao *et al.* [21] in which their results primarily showed more causal connectivities within the contralateral hemisphere, whereas interactions between

the two hemispheres are less observed. Our findings highlighted that the dynamic hemispherical lateralization during MI is characterized with the dominated role of contralateral SMA to serve as the causal hub node to exert information on other activated areas including those areas spanning across two hemispheres. In essence, this is in line with the activated map largely located within the contralateral primary motor areas during MI of hand actions [21], [60], [80]. In addition, such time-varying connectivity patterns of SMA are in accordance with its fundamental functions that are involved in action monitoring [81], [82], including motor initiation and inhibition, selection of actions, and motor planning [83], [84]. In a recent study, Bonini *et al.* [81] further revealed that SMA plays a leading role in evaluating successful and erroneous actions using the intracerebral electroencephalography (iEEG). Thus, we suggested that SMA acting as a 'causal outflow hub' is fundamental for assessing ongoing actions and detecting errors. At the same time, these casual connections also implied that both SMAs may dynamically modulate the intended action (i.e., imagined hand action) and suppress the unintended action (i.e., avoid executing hand action) during the current MI task. In fact, several previous studies had consistently demonstrated that effective connectivity (direction and strength) between SMA and M1 is modulated to adapt and optimize motor behavior [61], [73], [81].

F. DIFFERENCES OF TIME-VARYING NETWORKS BETWEEN LEFT- AND RIGHT-HAND MI

Though a similar causal outflow/inflow source and contralateralization connectivity pattern could be observed, there are actually some differences in the time-varying networks for the two MI tasks. The first difference is that the causal influence that the right hemisphere exerted on the left hemisphere during left-hand MI is much stronger than that the left hemisphere exerted on right hemisphere during right-hand MI for the right-handed subjects. These findings provided a novel avenue to understand the left hemisphere-dominant phenomenon during MI for the right-handed subjects. This left hemisphere-dominance occurred in the middle and later stages of MI (see Fig. 6e). Because the participants in our study were right-handed, the long experience of using right hand may have formed an optimized and specific circuit in the left hemisphere. Therefore, more coordinated interactions among activated regions may be needed when the right-handed subjects perform the left-hand MI task. Such interactions may facilitate generation of a compensable function for processing task related information. In a previous study, Rogers *et al.* [85] reported a left-hemisphere-dominant phenomenon for right-handed participants during unilateral finger movement. Using conditional granger causality analysis, Gao *et al.* [21] found that more regions within the left hemisphere were modulated during the left-hand MI. In fact, the time-varying in- and out-degrees consistently demonstrated such left lateralization for right-handed subjects.

The second difference is that the left PMA played a key role in modulating the dynamic network during right-hand MI compared to the role of right PMA during left-hand MI, especially in the early MI processes and last two states. Several studies had reported that PMA (including dorsal and ventral premotor areas) is involved in motor planning and action selection [54], [57], [86], [87]. In a previous study by Cisek and Kalaska [86], it was reported that the activation of the dorsal PMA of monkeys might contribute to predicting the directionality of forthcoming movement based on abstract visual cues and did not require the actor to be in view. By using the intracortical stimulation, Dum and Strick [88] found that PMA is a major source of input to M1 that is associated with the generation and control of hand movements. In our study, we found that there exists a causal influence from the left PMA to right M1 in the right MI task. Moreover, in a recent study, Ohbayashi *et al.* [89] demonstrated that the interaction between PMA and M1 guided the performance of internally generated sequences. Thus, we suggest that the interactions between the left PMA and other regions, such as the right M1, facilitate a response to abstract visual cues that instruct a task to be performed [86], guiding the performance of the current right-hand MI task. The different roles of PMA between the two MI tasks may account for the fact that it is easier for the right-handed subjects to perform the right-hand MI task than the left-hand MI task. These findings may serve as an important marker to distinguish between two MI conditions, which helps to optimize the BCI control system and facilitates better understanding of the neural mechanism of MI.

G. TIME-VARYING NETWORK PROPERTIES DURING THE LEFT- AND RIGHT-HAND MI

The networks mentioned above showed the time-varying topologies during MI tasks, and the network topologies could be quantitatively reflected by the corresponding network properties. Thus, we further employed graph analysis to characterize the temporal evolution of these interactions among activated regions. In this study, four commonly used weighted network properties were calculated for each subject for each state. As shown in Fig. 5, in both MI tasks, our results showed that the network efficiency is gradually increased (i.e., shorter L and higher C, Ge, and Le) at the states from cue to 5, followed by a relatively stable network efficiency. The temporal evolution of the network efficiency is consistent with the human brain's cognitive processes, such as the motor execution [53]. During the first five states, when a salient visual cue information was input, the left aIns acts as a prominent node to drive other regions within the network, which is in line with the function of the left aIns that may have a more prominent role in evaluating the need to implement subsequent behavioral adaptations [24]. Thus, the gradually increased network efficiency in the earlier MI stages indicated that the brain was optimizing the network resources and adjusting the network interaction to effectively respond to the current task demand. As the MI tasks progress into later stages, SMAs involved in guiding and monitoring motor action become the major causal outflow node, and the corresponding network pattern

is kept relatively stable, resulting in stable network properties in these MI periods. Moreover, the high network efficiency in the later stages implied that the brain has completed the optimization of the network.

In addition, we also found that the network efficiency of the right-hand MI task is higher than that of the left-hand MI task in the earlier MI stages, which may also infer that it is easier to perform the right-hand MI task for the right-handed subjects. In addition to the network properties, we also calculated the degree of nodes for each state. We found that the left aIns and right SMA have relatively high out-degree and that the left IPL and right aIns have relatively high in-degree during the left-hand MI task, whereas the left aIns, PMA and SMA have relatively high out-degrees and the right aIns has relatively high in-degree during the right-hand MI task. These results consistently suggested that these regions, as important causal targets, modulate the reconfiguration of time-varying networks for different MI tasks.

V. CONCLUSION

In our study, we applied ADTF to fMRI data to track the time-varying effective connectivity patterns among activated regions during MIs. This method can not only capture changes of temporal evolution of network patterns but also estimate the information flow of the network. The following conclusions can be drawn from the time-varying MI networks: 1) the left aIns, contralateral M1, and contralateral SMA corresponding to the performing hand are important causal sources for completing the specific MI task. 2) The casual source switching indicates there exists a hierarchical organization during MI, for example, in the early stages of MI (i.e., 4 TRs $=$ 8 s); the left aIns and contralateral M1 act as important casual in-/outflow nodes to modulate the patterns of networks for both MI tasks. As time goes by, the contralateral SMA separately becomes the new causal source for left- and right-hand MI tasks. 3) The lateralization of left- and right-hand MI occurred not only in neural activity but also in the connectivity modulated by the causal source, such as the contralateral SMA. Furthermore, graph theory analysis further characterized the temporal evolution of these interactions among activated regions during MI. Taken together, these findings deepen our understanding of dynamic information processing in motor imagery from the perspective of a time-varying network.

REFERENCES

[1] A. Guillot, F. Di Rienzo, T. Macintyre, A. Moran, and C. Collet, "Imagining is not doing but involves specific motor commands: A review of experimental data related to motor inhibition," *Frontiers Hum. Neurosci.*, vol. 6, p. 247, Sep. 2012.
[2] C. Pandarinath *et al.*, "High performance communication by people with paralysis using an intracortical brain-computer interface," *eLIFE*, vol. 6, p. e18554, Feb. 2017.
[3] F. Pichiorri *et al.*, "Brain–computer interface boosts motor imagery practice during stroke recovery," *Ann. Neurol.*, vol. 77, no. 5, pp. 851–865, 2015.
[4] K. R. Ridderinkhof and M. Brass, "How kinesthetic motor imagery works: A predictive-processing theory of visualization in sports and motor expertise," *J. Physiol. Paris*, vol. 109, pp. 53–63, Feb./Jun. 2015.
[5] Y. Li *et al.*, "An EEG-based BCI system for 2-D cursor control by combining mu/beta rhythm and P300 potential," *IEEE Trans. Biomed. Eng.*, vol. 57, no. 10, pp. 2495–2505, Oct. 2010.
[6] J. Long, Y. Li, T. Yu, and Z. Gu, "Target selection with hybrid feature for BCI-based 2-D cursor control," *IEEE Trans. Biomed. Eng.*, vol. 59, no. 1, pp. 132–140, Jan. 2012.
[7] J. Long, Y. Li, H. Wang, T. Yu, J. Pan, and F. Li, "A hybrid brain computer interface to control the direction and speed of a simulated or real wheelchair," *IEEE Trans. Neural Syst. Rehabil. Eng.*, vol. 20, no. 5, pp. 720–729, Sep. 2012.
[8] R. Zhang *et al.*, "Efficient resting-state EEG network facilitates motor imagery performance," *J. Neural Eng.*, vol. 12, no. 6, p. 066024, Dec. 2015.
[9] T. Aflalo *et al.*, "Decoding motor imagery from the posterior parietal cortex of a tetraplegic human," *Science*, vol. 348, pp. 906–910, May 2015.
[10] T. Zhang *et al.*, "Structural and functional correlates of motor imagery BCI performance: Insights from the patterns of fronto-parietal attention network," *NeuroImage*, vol. 134, pp. 475–485, Jul. 2016.
[11] C. Zich, S. Debener, C. Kranczioch, M. G. Bleichner, I. Gutberlet, and M. De Vos, "Real-time EEG feedback during simultaneous EEG–fMRI identifies the cortical signature of motor imagery," *NeuroImage*, vol. 114, pp. 438–447, Jul. 2015.
[12] S. Hétu *et al.*, "The neural network of motor imagery: An ALE meta-analysis," *Neurosci. Biobehav. Rev.*, vol. 37, pp. 930–949, Jun. 2013.
[13] S. L. Bressler and V. Menon, "Large-scale brain networks in cognition: Emerging methods and principles," *Trends Cogn. Sci.*, vol. 14, pp. 277–290, Jun. 2010.
[14] B. Mišić and O. Sporns, "From regions to connections and networks: New bridges between brain and behavior," *Current Opinion Neurobiol.*, vol. 40, pp. 1–7, Oct. 2016.
[15] S. Smith, "Linking cognition to brain connectivity," *Nature Neurosci.*, vol. 19, pp. 7–9, Dec. 2015.
[16] M. Ahmadlou, H. Adeli, and A. Adeli, "Spatiotemporal analysis of relative convergence of EEGs reveals differences between brain dynamics of depressive women and men," *Clin. EEG Neurosci.*, vol. 44, pp. 175–181, Jul. 2013.
[17] M. Ahmadlou, H. Adeli, and A. Adeli, "Graph theoretical analysis of organization of functional brain networks in ADHD," *Clin. EEG Neurosci.*, vol. 43, no. 1, pp. 5–13, 2012.
[18] Z. K. Gao, Q. Cai, Y. X. Yang, N. Dong, and S. S. Zhang, "Visibility graph from adaptive optimal kernel time-frequency representation for classification of epileptiform EEG," *Int. J. Neural Syst.*, vol. 27, no. 4, p. 1750005, Jun. 2017.
[19] B. Biswal, F. Z. Yetkin, V. M. Haughton, and J. S. Hyde, "Functional connectivity in the motor cortex of resting human brain using echo-planar MRI," *Magn. Reson. Med.*, vol. 34, pp. 537–541, Oct. 1995.
[20] M. Kamiński, M. Ding, W. A. Truccolo, and S. L. Bressler, "Evaluating causal relations in neural systems: Granger causality, directed transfer function and statistical assessment of significance," *Biol. Cybern.*, vol. 85, pp. 145–157, Aug. 2001.
[21] Q. Gao, X. Duan, and H. Chen, "Evaluation of effective connectivity of motor areas during motor imagery and execution using conditional Granger causality," *NeuroImage*, vol. 54, pp. 1280–1288, Jan. 2011.
[22] A. Solodkin, P. Hlustik, E. E. Chen, and S. L. Small, "Fine modulation in network activation during motor execution and motor imagery," *Cerebral Cortex*, vol. 14, pp. 1246–1255, Nov. 2004.
[23] M. D. Fox, A. Z. Snyder, J. L. Vincent, M. Corbetta, D. C. Van Essen, and M. E. Raichle, "The human brain is intrinsically organized into dynamic, anticorrelated functional networks," *Proc. Nat. Acad. Sci. USA*, vol. 102, pp. 9673–9678, May 2005.
[24] J. Späti *et al.*, "Functional lateralization of the anterior insula during feedback processing," *Hum. Brain Mapping*, vol. 35, pp. 4428–4439, Sep. 2014.
[25] R. P. Monti, P. Hellyer, D. Sharp, R. Leech, C. Anagnostopoulos, and G. Montana, "Estimating time-varying brain connectivity networks from functional MRI time series," *Neuroimage*, vol. 103, pp. 427–443, Dec. 2014.
[26] S. E. Petersen and O. Sporns, "Brain networks and cognitive architectures," *Neuron*, vol. 88, pp. 207–219, Oct. 2015.
[27] D. L. Zabelina and J. R. Andrews-Hanna, "Dynamic network interactions supporting internally-oriented cognition," *Current Opinion Neurobiol.*, vol. 40, pp. 86–93, Oct. 2016.
[28] O. Sporns, "Contributions and challenges for network models in cognitive neuroscience," *Nature Neurosci.*, vol. 17, pp. 652–660, Mar. 2014.

[29] V. D. Calhoun, R. Miller, G. Pearlson, and T. Adalı, "The chronnectome: Time-varying connectivity networks as the next frontier in fMRI data discovery," *Neuron*, vol. 84, pp. 262–274, Oct. 2014.

[30] E. A. Allen, E. Damaraju, S. M. Plis, E. B. Erhardt, T. Eichele, and V. D. Calhoun, "Tracking whole-brain connectivity dynamics in the resting state," *Cerebral Cortex*, vol. 24, pp. 663–676, Mar. 2014.

[31] E. Damaraju *et al.*, "Dynamic functional connectivity analysis reveals transient states of dysconnectivity in schizophrenia," *NeuroImage, Clin.*, vol. 5, pp. 298–308, Jul. 2014.

[32] G. Deshpande, S. LaConte, G. A. James, S. Peltier, and X. Hu, "Multivariate Granger causality analysis of fMRI data," *Hum. Brain Mapping*, vol. 30, pp. 1361–1373, Apr. 2009.

[33] X. Liu and J. H. Duyn, "Time-varying functional network information extracted from brief instances of spontaneous brain activity," *Proc. Nat. Acad. Sci. USA*, vol. 110, no. 11, pp. 4392–4397, 2013.

[34] A. Omidvarnia, G. Azemi, B. Boashash, J. M. O'Toole, P. B. Colditz, and S. Vanhatalo, "Measuring time-varying information flow in scalp EEG signals: Orthogonalized partial directed coherence," *IEEE Trans. Biomed. Eng.*, vol. 61, no. 3, pp. 680–693, Mar. 2014.

[35] G. Plomp, C. Quairiaux, C. M. Michel, and L. Astolfi, "The physiological plausibility of time-varying Granger-causal modeling: Normalization and weighting by spectral power," *NeuroImage*, vol. 97, pp. 206–216, Aug. 2014.

[36] C. Wilke, L. Ding, and B. He, "Estimation of time-varying connectivity patterns through the use of an adaptive directed transfer function," *IEEE Trans. Biomed. Eng.*, vol. 55, no. 11, pp. 2557–2564, Nov. 2008.

[37] W.-Y. Hsu, "Single-trial motor imagery classification using asymmetry ratio, phase relation, wavelet-based fractal, and their selected combination," *Int. J. Neural Syst.*, vol. 23, no. 2, p. 1350007, 2013.

[38] G. Rodríguez-Bermúdez, P. J. García-Laencina, and J. Roca-Dorda, "Efficient automatic selection and combination of eeg features in least squares classifiers for motor imagery brain–computer interfaces," *Int. J. Neural Syst.*, vol. 23, no. 4, p. 1350015, 2013.

[39] S. B. Samdin, C.-M. Ting, S.-H. Salleh, M. Hamedi, and A. B. M. Noor, "Estimating dynamic cortical connectivity from motor imagery EEG using KALMAN smoother & EM algorithm," in *Proc. IEEE Workshop Stat. Signal Process. (SSP)*, Jun./Jul. 2014, pp. 181–184.

[40] F. Li *et al.*, "The time-varying networks in P300: A task-evoked EEG study," *IEEE Trans. Neural Syst. Rehabil. Eng.*, vol. 24, no. 7, pp. 725–733, Jul. 2016.

[41] S. M. Smith *et al.*, "Network modelling methods for FMRI," *NeuroImage*, vol. 54, pp. 875–891, Jan. 2011.

[42] R. N. Spreng, J. Sepulcre, G. R. Turner, W. D. Stevens, and D. L. Schacter, "Intrinsic architecture underlying the relations among the default, dorsal attention, and frontoparietal control networks of the human brain," *J. Cogn. Neurosci.*, vol. 25, pp. 74–86, Jan. 2013.

[43] D. Vatansever, D. K. Menon, A. E. Manktelow, B. J. Sahakian, and E. A. Stamatakis, "Default mode network connectivity during task execution," *Neuroimage*, vol. 122, pp. 96–104, Nov. 2015.

[44] L. Astolfi *et al.*, "Tracking the time-varying cortical connectivity patterns by adaptive multivariate estimators," *IEEE Trans. Biomed. Eng.*, vol. 55, no. 3, pp. 902–913, Mar. 2008.

[45] G. Deshpande, S. LaConte, S. Peltier, and X. Hu, "Directed transfer function analysis of fMRI data to investigate network dynamics," in *Proc. Int. Conf. IEEE Eng. Med. Biol. Soc.*, vol. 1, Aug./Sep. 2006, pp. 671–674.

[46] T. Milde *et al.*, "A new Kalman filter approach for the estimation of high-dimensional time-variant multivariate AR models and its application in analysis of laser-evoked brain potentials," *Neuroimage*, vol. 50, pp. 960–969, Apr. 2010.

[47] L. Hu, Z. G. Zhang, and Y. Hu, "A time-varying source connectivity approach to reveal human somatosensory information processing," *Neuroimage*, vol. 62, pp. 217–228, Aug. 2012.

[48] H. Akaike, "A new look at the statistical model identification," *IEEE Trans. Autom. Control*, vol. AC-19, no. 6, pp. 716–723, Dec. 1974.

[49] M. Rubinov and O. Sporns, "Complex network measures of brain connectivity: Uses and interpretations," *NeuroImage*, vol. 52, no. 3, pp. 1059–1069, 2010.

[50] E. Bullmore and O. Sporns, "Complex brain networks: Graph theoretical analysis of structural and functional systems," *Nature Rev. Neurosci.*, vol. 10, no. 3, pp. 186–198, Mar. 2009.

[51] J.-R. Ding *et al.*, "Altered functional and structural connectivity networks in psychogenic non-epileptic seizures," *PLoS one*, vol. 8, no. 5, p. e63850, 2013.

[52] F. Liu *et al.*, "Dynamic functional network connectivity in idiopathic generalized epilepsy with generalized tonic–clonic seizure," *Hum. Brain Mapping*, vol. 38, no. 2, pp. 957–973, 2017.

[53] F. De Vico Fallani *et al.*, "Cortical network dynamics during foot movements," *Neuroinformatics*, vol. 6, no. 1, pp. 23–34, 2008.

[54] N. Li, K. Daie, K. Svoboda, and S. Druckmann, "Robust neuronal dynamics in premotor cortex during motor planning," *Nature*, vol. 532, pp. 459–464, Apr. 2016.

[55] A. Ekstrom, "How and when the fMRI BOLD signal relates to underlying neural activity: The danger in dissociation," *Brain Res. Rev.*, vol. 62, pp. 233–244, Mar. 2010.

[56] T. O. Laumann *et al.*, "On the stability of BOLD fMRI correlations," *Cerebral Cortex*, vol. 27, pp. 4719–4732, Oct. 2017.

[57] E. Hoshi and J. Tanji, "Distinctions between dorsal and ventral premotor areas: Anatomical connectivity and functional properties," *Current Opinion Neurobiol.*, vol. 17, pp. 234–242, Apr. 2007.

[58] R. Grush, "The emulation theory of representation: Motor control, imagery, and perception," *Behav. Brain Sci.*, vol. 27, pp. 377–396, Jun. 2004.

[59] B. D. Berman, S. G. Horovitz, G. Venkataraman, and M. Hallett, "Self-modulation of primary motor cortex activity with motor and motor imagery tasks using real-time fMRI-based neurofeedback," *Neuroimage*, vol. 59, no. 2, pp. 917–925, Jan. 2012.

[60] S. Halder *et al.*, "Neural mechanisms of brain–computer interface control," *Neuroimage*, vol. 55, pp. 1779–1790, Apr. 2011.

[61] C. H. Kasess, C. Windischberger, R. Cunnington, R. Lanzenberger, L. Pezawas, and E. Moser, "The suppressive influence of SMA on M1 in motor imagery revealed by fMRI and dynamic causal modeling," *NeuroImage*, vol. 40, pp. 828–837, Apr. 2008.

[62] S. M. Nelson, N. U. Dosenbach, A. L. Cohen, M. E. Wheeler, B. L. Schlaggar, and S. E. Petersen, "Role of the anterior insula in task-level control and focal attention," *Brain Struct. Funct.*, vol. 214, pp. 669–680, Jun. 2010.

[63] V. Menon and L. Q. Uddin, "Saliency, switching, attention and control: A network model of insula function," *Brain Struct. Funct.*, vol. 214, pp. 655–667, Jun. 2010.

[64] L. J. Chang, T. Yarkoni, M. W. Khaw, and A. G. Sanfey, "Decoding the role of the insula in human cognition: Functional parcellation and large-scale reverse inference," *Cerebral Cortex*, vol. 23, pp. 739–749, Mar. 2013.

[65] T. Singer, H. D. Critchley, and K. Preuschoff, "A common role of insula in feelings, empathy and uncertainty," *Trends Cognit. Sci.*, vol. 13, pp. 334–340, Aug. 2009.

[66] M. Jabbi, J. Bastiaansen, and C. Keysers, "A common anterior insula representation of disgust observation, experience and imagination shows divergent functional connectivity pathways," *PLoS one*, vol. 3, no. 8, p. e2939, 2008.

[67] L. Q. Uddin, "Salience processing and insular cortical function and dysfunction," *Nature Rev. Neurosci.*, vol. 16, pp. 55–61, Nov. 2014.

[68] L. Q. Uddin, K. S. Supekar, S. Ryali, and V. Menon, "Dynamic reconfiguration of structural and functional connectivity across core neurocognitive brain networks with development," *J. Neurosci.*, vol. 31, no. 50, pp. 18578–18589, 2011.

[69] A. D. Craig, "How do you feel? Interoception: The sense of the physiological condition of the body," *Nature Rev. Neurosci.*, vol. 3, pp. 655–666, Aug. 2002.

[70] N. U. Dosenbach *et al.*, "Distinct brain networks for adaptive and stable task control in humans," *Proc. Nat. Acad. Sci. USA*, vol. 104, no. 26, pp. 11073–11078, 2007.

[71] J. Munzert, B. Lorey, and K. Zentgraf, "Cognitive motor processes: The role of motor imagery in the study of motor representations," *Brain Res. Rev.*, vol. 60, pp. 306–326, May 2009.

[72] B. Pelgrims, N. Michaux, E. Olivier, and M. Andres, "Contribution of the primary motor cortex to motor imagery: A subthreshold TMS study," *Hum. Brain Mapping*, vol. 32, pp. 1471–1482, Sep. 2011.

[73] E. Raffin, J. Mattout, K. T. Reilly, and P. Giraux, "Disentangling motor execution from motor imagery with the phantom limb," *Brain*, vol. 135, pp. 582–595, Feb. 2012.

[74] L. R. Hochberg *et al.*, "Neuronal ensemble control of prosthetic devices by a human with tetraplegia," *Nature*, vol. 442, pp. 164–171, Jul. 2006.

[75] S. Bajaj, A. J. Butler, D. Drake, and M. Dhamala, "Brain effective connectivity during motor-imagery and execution following stroke and rehabilitation," *NeuroImage Clin.*, vol. 8, pp. 572–582, Jun. 2015.

[76] T. Hanakawa, M. A. Dimyan, and M. Hallett, "Motor planning, imagery, and execution in the distributed motor network: A time-course study with functional MRI," *Cerebral Cortex*, vol. 18, pp. 2775–2788, Dec. 2008.
[77] N. Arai, M.-K. Lu, Y. Ugawa, and U. Ziemann, "Effective connectivity between human supplementary motor area and primary motor cortex: A paired-coil TMS study," *Exp. Brain Res.*, vol. 220, pp. 79–87, Jul. 2012.
[78] D. N. Pandya and L. A. Vignolo, "Intra- and interhemispheric projections of the precentral, premotor and arcuate areas in the rhesus monkey," *Brain Res.*, vol. 26, pp. 217–233, Mar. 1971.
[79] N. Arai *et al.*, "State-dependent and timing-dependent bidirectional associative plasticity in the human SMA-M1 network," *J. Neurosci.*, vol. 31, no. 43, pp. 15376–15383, 2011.
[80] B. Blankertz *et al.*, "Neurophysiological predictor of SMR-based BCI performance," *Neuroimage*, vol. 51, pp. 1303–1309, Jul. 2010.
[81] F. Bonini, B. Burle, C. Liégeois-Chauvel, J. Régis, P. Chauvel, and F. Vidal, "Action monitoring and medial frontal cortex: Leading role of supplementary motor area," *Science*, vol. 343, no. 6173, pp. 888–891, 2014.
[82] P. Nachev, C. Kennard, and M. Husain, "Functional role of the supplementary and pre-supplementary motor areas," *Nature Rev. Neurosci.*, vol. 9, pp. 856–869, Oct. 2008.
[83] C. F. Lima, S. Krishnan, and S. K. Scott, "Roles of supplementary motor areas in auditory processing and auditory imagery," *Trends Neurosci.*, vol. 39, no. 8, pp. 527–542, Aug. 2016.
[84] P. Y. Chauvel, M. Rey, P. Buser, and J. Bancaud, "What stimulation of the supplementary motor area in humans tells about its functional organization," *Adv. Neurol.*, vol. 70, pp. 199–209, Jun. 1996.
[85] B. P. Rogers, J. D. Carew, and M. E. Meyerand, "Hemispheric asymmetry in supplementary motor area connectivity during unilateral finger movements," *Neuroimage*, vol. 22, pp. 855–859, Jun. 2004.
[86] P. Cisek and J. F. Kalaska, "Neural correlates of mental rehearsal in dorsal premotor cortex," *Nature*, vol. 431, pp. 993–996, Oct. 2004.
[87] J. Grèzes and J. Decety, "Functional anatomy of execution, mental simulation, observation, and verb generation of actions: A meta-analysis," *Hum. Brain Mapping*, vol. 12, no. 1, pp. 1–19, 2001.
[88] R. P. Dum and P. L. Strick, "Frontal lobe inputs to the digit representations of the motor areas on the lateral surface of the hemisphere," *J. Neurosci.*, vol. 25, pp. 1375–1386, Feb. 2005.
[89] M. Ohbayashi, N. Picard, and P. L. Strick, "Inactivation of the dorsal premotor area disrupts internally generated, but not visually guided, sequential movements," *J. Neurosci.*, vol. 36, pp. 1971–1976, Feb. 2016.

TAO ZHANG received the Ph.D. degree in biomedical engineering from the University of Electronic Science and Technology of China, Chengdu, China, in 2017. His research interests include magnetic resonance imaging, electroencephalogram, motor imagery, machine learning, and brain–computer Interface.

MENGCHEN LI received the M.S. degree in biomedical engineering from the University of Electronic Science and Technology of China, Chengdu, China, in 2017. His research interests include magnetic resonance imaging, machine learning, and brain–computer Interface.

LI ZHANG received the M.A. degree in linguistics and applied linguistics from Hunan University, Changsha, China, in 2012. She is currently an Instructor with the Chengdu Institute, Sichuan International Studies University, Chengdu, China. Her research interests include syntax, semantics, English teaching, and English literature.

BHARAT BISWAL is currently an Internationally Renowned Researcher recognized for mapping the brain's activity, the Chair of the Department of Biomedical Engineering, and a PI at the University of Electronic Science and Technology of China. He joined the Newark College of Engineering as a Professor. His impact is reflected in the fact that he is an ISI highly cited researcher in neuroscience and behavior. He has authored some of the most highly cited papers in clinical imaging since 2014. He has authored and co-authored 150 articles appearing in peer-reviewed journals. His work has appeared in high-profile journals in psychology, neuroscience, and engineering, including *The Journal of Neuroscience*, *Proceedings of the National Academy of Sciences*, *NeuroImage*, *Cerebral Cortex*, and *Human Brain Mapping*.

DEZHONG YAO is currently a Changjiang Professor with the University of Electronic Science and Technology of China and the Director of the Key Laboratory for NeuroInformation, Ministry of Education of China. His major research area is in methods on electroencephalogram (EEG), magnetic resonance imaging, and EEG+fMRI, with applications to brain–computer interface, epilepsy, and music. He proposed a method of EEG zero reference (Reference Electrode Standardization Technique), which is adopted in various studies around the world. He is a fellow of the American Academy of Medical Bioengineering.

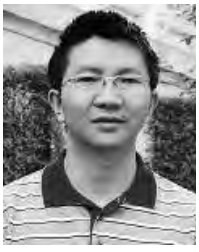

PENG XU received the B.S and Ph.D. degrees in biomedical engineering from the University of Electronic Science and Technology of China (UESTC), Chengdu, China, in 2000 and 2006, respectively. He held a post-doctoral position at the Neural Systems and Dynamics Laboratory, University of California, Los Angeles, from 2007 to 2009. He is currently a Professor with the School of Life Science and Technology, UESTC.